On the Behavior of Koch Island Fractal Boundary Microstrip Patch Antenna

Carmen Borja, *Student Member, IEEE,* and Jordi Romeu, *Member, IEEE*

Abstract—The properties of the Koch island fractal boundary microstrip patch antenna are presented. The behavior at the fundamental mode and the existence of high-order modes that exhibit localized current density distributions is discussed. The main features are the size reduction of the patch resonating at the fundamental frequency when compared to Euclidean-shaped patches, and the application of localized modes in designing microstrip patch antennas with directive patterns.

Index Terms—Antennas, fractals, microstrip antennas.

I. INTRODUCTION

FRACTAL shaped antennas exhibit some interesting features that stem from their geometrical properties. The self-similarity of certain fractal structures results in a multiband behavior of self-similar fractal antennas and frequency-selective surfaces (FSS) [1]–[3]. On the other hand, the high convoluted shape of certain fractals allows to reduce the overall volume occupied by a resonant element [4], [5]. These properties have been useful in designing multiband antennas and FSS, and in reducing the size of certain antennas [6]. The physical construction of the fractal is not possible. Only objects with a limited number of iterations can be built. These objects are usually referred to as prefractals. Although complex objects with similar properties of the prefractals could be defined, the use of fractal geometries has the advantage that irregular complex objects can be described in a well-defined geometrical framework. In this way, the definition of the geometry, and even its numerical analysis can be greatly simplified [7].

In this paper, the properties of a fractal boundary microstrip antenna will be presented and discussed. The properties of fractal resonators have been a subject of theoretical and experimental studies [8]–[11]. The physical problem is often referred to in the literature as the determination of the "fractal drum" vibration modes. A fractal drum is the simplest example of a surface fractal resonator, where a vibrating membrane is bounded by a fractal curve. A more complex structure is the "mass fractal." In the latter case, the mass density of the vibrating membrane is defined by a fractal. Therefore, two types of fractal resonators are considered in the literature: mass fractals and surface fractals. Their vibration modes are named
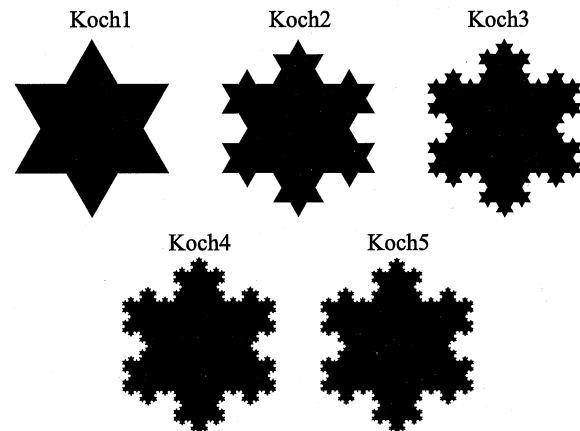
The authors are with the Department of Signal Theory and Communications, Telecommunication Engineering School of the Universitat Politecnica de Catalunya, and Centre Tecnològic de Telecomunicacions de Catalunya (CTTC), Barcelona, Spain (e-mail: romeu@tsc.upc.es).

Fig. 1. Geometry of the Koch island or "snowflake" prefractal for increasing number of iterations. The geometry can be obtained by replacing each of the sides of an equilateral triangle by a Koch curve.

"fractons" and "fractinos," respectively, [9]. The vibration modes of fractal drums exhibit some interesting properties such as the existence of localized modes. In these localized modes, the vibration is strongly localized in certain parts of the membrane. These vibrational states are obtained after the solution of the Helmholtz equation with the appropriate boundary condition. For surface fractals, a distinction is made between Neumann and Dirichtlet fractinos according to the boundary condition that is applied.

Microstrip patch antennas can be modeled in a first approximation as a cavity. For a microstrip patch antenna of electrically small height h, the field distribution can be found with very good accuracy from the eigenfunctions of the Helmholtz equation subject to the Neumann boundary condition. Therefore, it is expected that fractal boundary microstrip antennas will exhibit vibration modes similar to the ones of the fractal drum. While some preliminary results were discussed by the authors in [12]–[14], this paper will provide an in-depth insight to the behavior of the fractal boundary microstrip patch antena in the fundamental mode and in the localized modes. In Section II, a description of the geometry of the Koch island or "snowflake" microstrip patch antenna is presented. In Section III, the behavior of the antenna in the fundamental mode is discussed. The resonant frequency, the quality factor Q, and their dependence on the number of iterations of the prefractal is discussed. The existence of localized modes and their application in synthesizing directive patterns is presented in Section IV. In this paper, by directive pattern is meant a radiation pattern with a noticeable increment of directivity with comparison to the pattern at the fundamental mode. In Section V, it is shown that localized
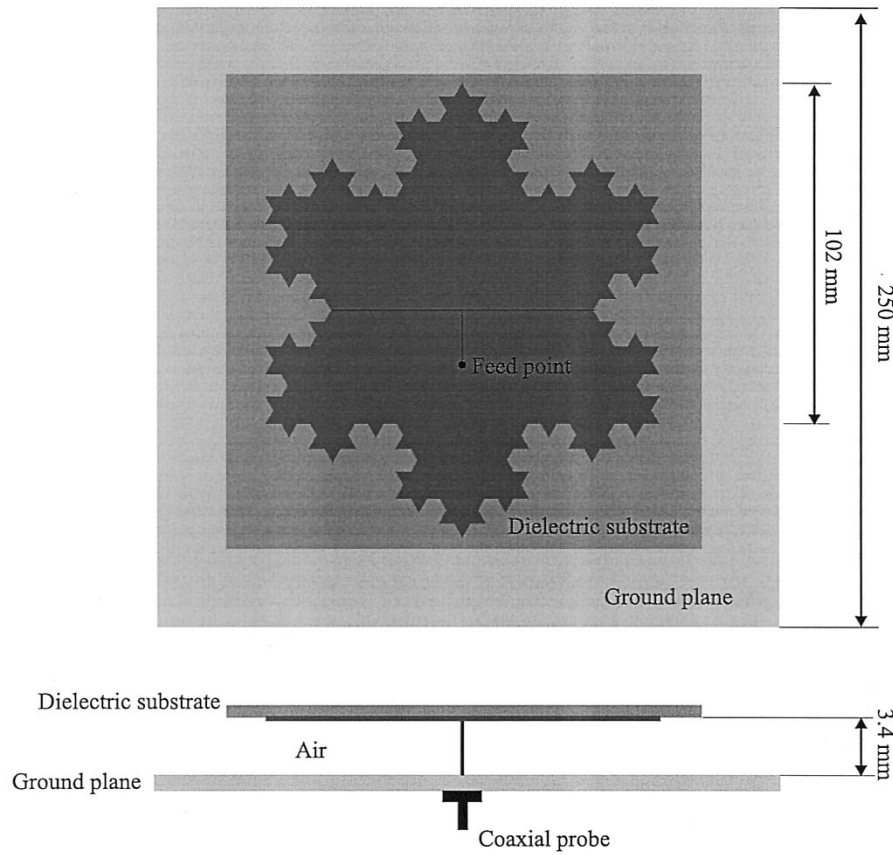
Fig. 2. Measured and simulated configurations for the three-iteration version of the Koch island patch. For the simulations, an infinite ground plane lossless case is considered.

modes that result in directive patterns can be obtained in other fractal boundary antennas. The main results are summarized in the final section.

II. GEOMETRY OF KOCH ISLAND FRACTAL BOUNDARY MICROSTRIP PATCH ANTENNAS

The basic geometry that is analyzed throughout this paper is the Koch island or snowflake prefractal. This geometry is obtained by replacing the sides of an equilateral triangle by a Koch curve. In Fig. 1, the Koch island fractal at different iteration stages is shown. At each new iteration k the area of the island increases. Let A_k be the area at iteration k, then the area of the next iteration can be computed as

$$A_{k+1} = A_k + \frac{\sqrt{3}}{12} \left(\frac{4}{9} \right)^{k-1} \cdot a^2 \qquad (1)$$

where a is the side of the initial triangle that has an area $A_0 = (\sqrt{3}/4)a^2$. The geometric series given by (1) converges to

$$A = \frac{2}{5} \sqrt{3} a^2. \qquad (2)$$

All the iterations are circumscribed inside a circumference of radius $r = \sqrt{3}a/3$. On the other hand, the perimeter increases

at each new iteration. The overall perimeter for iteration k is given by

$$l_k = 3a \left(\frac{4}{3} \right)^k. \qquad (3)$$

For the fractal, an infinite perimeter bounding a finite area is obtained. Despite of the increasing irregularity of the boundary, the manufacturing process does not become more complex at each new iteration. The patch can be manufactured by standard photo-etching techniques. The fundamental limitation in building the antenna is given by the resolution of the photo-etching process. When the number of iterations is increased, the new added details in the structure cannot be resolved, and they are not reproduced in the manufactured element.

III. THE BEHAVIOR OF THE KOCH ISLAND FRACTAL PATCH AT THE FUNDAMENTAL MODE

There are two parameters of interest in the study of the behavior of the Koch island fractal patch antenna at the fundamental mode. These parameters are the resonant frequency and the quality factor Q. It is of special interest to compare the behavior of this antenna with equivalent Euclidean-shaped patches such as the circular-patch antenna.

In order to check the dependence of the resonant frequency of the fundamental mode on the number of iterations, the input impedance corresponding to the first five iterations
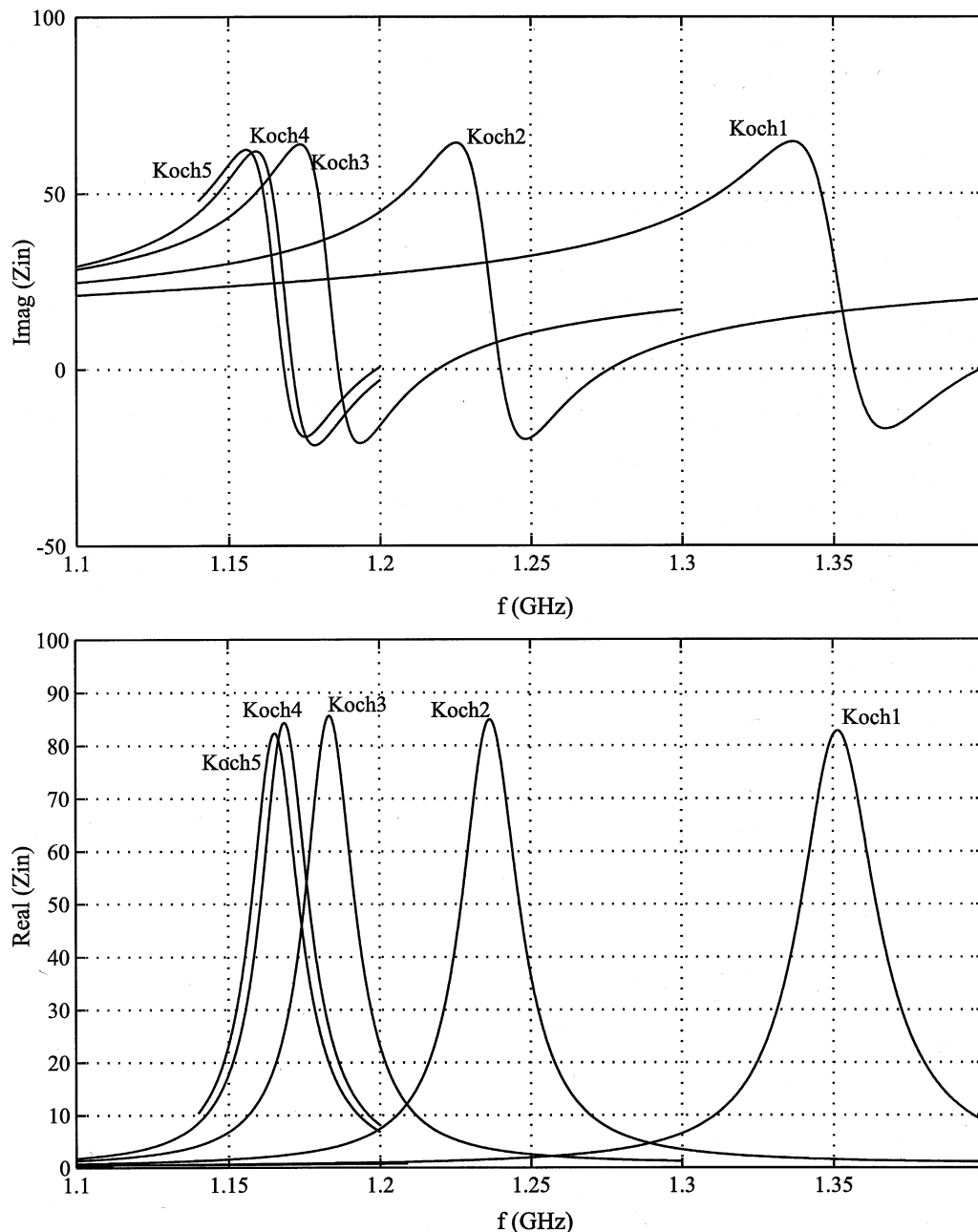
Fig. 3. The Koch island patch input impedance evolution for several fractal iterations. The plots show the simulated input resistance and reactance. At the resonance, an inductive reactive behavior due to the effect of the coaxial feed is observed. The resonant frequency decreases when the number of iterations increases.

of the Koch island microstrip patch antenna has been measured and analyzed. All numerical analysis in this paper has been done with the IE3D method of moments (MoM) code. The Koch patches are generated by an equilateral triangle whose side is 118.2 mm. They are printed on a glass fiber substrate (relative dielectric constant $\varepsilon_r = 4.17$ and 1.6-mm height). Fig. 2 displays the measured configuration for the three-iteration version of the Koch island patch. The printed metallic region is placed at 3.4 mm from the ground plane. The patches are fed by a coaxial probe, and the feed point is at the same location for all the patches and it is placed at 16.5 mm from the center of the patch. In order to have a well-defined linear polarization, the feed point has been chosen along

one of the symmetry axes of the patch. The exact location has been experimentally determined for optimum impedance matching. The simulated configuration is the same, but the ground plane is considered infinite.

The simulated input resistance and reactance of the five Koch island patches is plotted in Fig. 3. An interesting conclusion can be derived from the input parameter plot. The fundamental resonant frequency decreases when the number of iterations increases. Nevertheless, this effect is less important as the number of iterations increases. Thus, the difference between the Koch4 and Koch5 resonant frequencies is only 0.27%, which is a very small difference, while the difference between the Koch1 and Koch2 resonant frequencies is 9%.
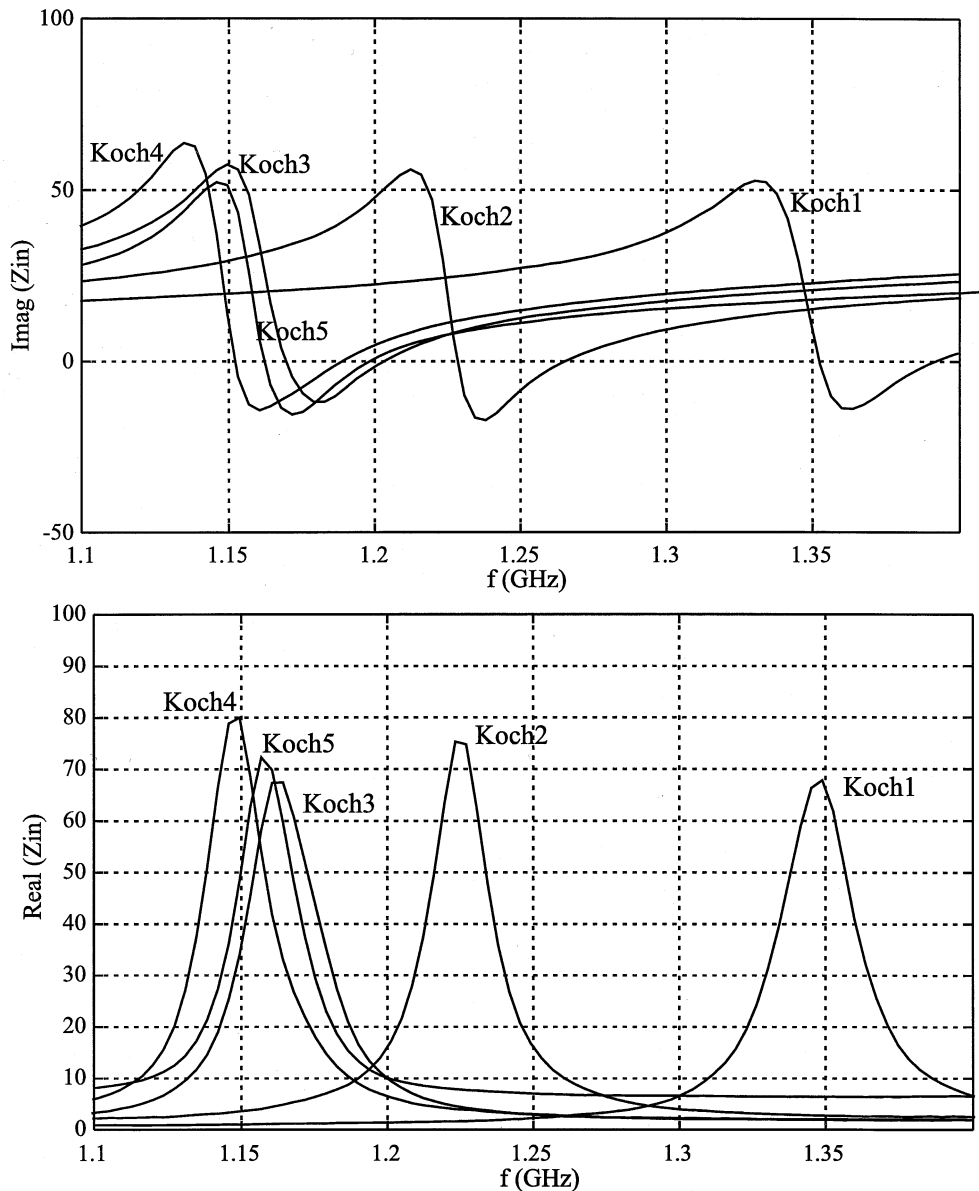
Fig. 4.   The Koch island patch input impedance evolution for several fractal iterations. The plots show the measured input resistance and reactance.

The measured input resistance and reactance for the five Koch island patches are displayed in Fig. 4. The resonant frequency also decreases when the number of iterations increases. However, at the fourth iteration, the measured resonant frequency is smaller than the measured at the fifth iteration. The difference between the measured resonant frequencies for the Koch4 and Koch5 patches is only 0.96%. As the difference between the resonant frequencies of the Koch4 and Koch5 patches is so small, they can be attributed to slight differences in the manufactured patches.

In order to show the frequency reduction when the number of iterations increases, Fig. 5 represents the measured and simulated frequency-reduction factor as a function of the iteration number. The reduction factor is defined with respect to the Koch1 patch resonant frequency. Fig. 5 also shows the area increment factor as a function of the iteration number, the area increment factor is defined also in relation to the Koch1 patch area.

It becomes apparent that for the Koch patches, the reduction of the resonant frequency follows the increment of the area when the number of iterations increase. In agreement with the results, the resonant frequency of the Koch5 patch can be reduced by a factor 1.17 compared to the Koch1 patch. Finally, it is worthwhile to note that a circular patch that circumscribes the Koch island has a resonant frequency of 1.19 GHz, that is, slightly higher than the resonant frequency of the Koch island patch antenna. Therefore, for a given volume occupied by the radiating element, a lower resonant frequency is obtained with the Koch island fractal patch in comparison to the circular patch. Moreover, the area of the Koch island fractal is 0.66 times smaller than the area of the circle that encloses it. This area reduction can be advantageous when material cost and mass reduction considerations are involved in the design.

It is also interesting to find the quality factor Q of the Koch island fractal boundary microstrip antenna, its dependence on
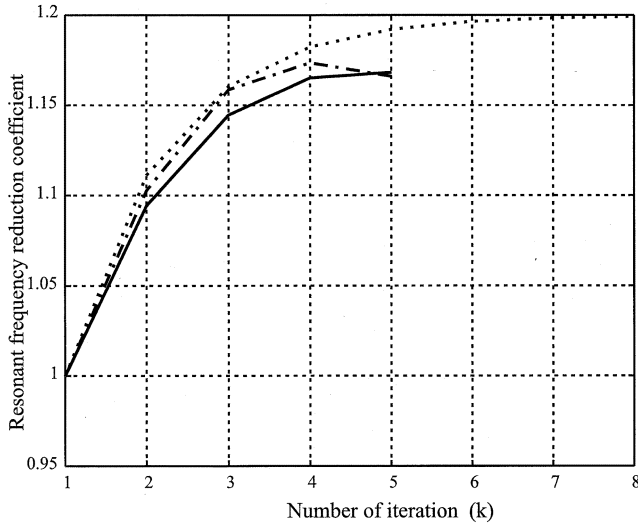
Fig. 5. The measured (dash-dot line) and simulated (solid line) frequency-reduction factor and the area increment factor (dotted line) as a function of the number of iterations, both parameters are defined with respect to the Koch1 patch.

TABLE I

FUNDAMENTAL RESONANT FREQUENCY AND QUALITY FACTOR OF THE KOCH AND EUCLIDEAN PATCHES WHEN ALL THE PATCHES HOLD THE SAME AREA

Parameter	Koch1	Koch2	Koch3	Koch4	Circular	Hexagonal
$f(GHz)$	1.78	1.71	1.69	1.66	2	2.03
Q_{Aitken}	24.3	27.8	27.2	25.4	12.3	17.3
Q_{Kajfez}	21.7	21.2	26.4	25.7	12.6	17.9

TABLE II

FUNDAMENTAL RESONANT FREQUENCY AND QUALITY FACTOR OF THE KOCH AND THE EUCLIDEAN PATCH WHEN ALL OF THEM EXHIBIT A SIMILAR RESONANT FREQUENCY

Geometry	Koch3	Koch5	Circular	Koch3	Koch5	Circular
Parameter	Meas.	Meas.	Meas.	Sim.	Sim.	Sim.
$f(GHz)$	1.19	1.17	1.19	1.2	1.17	1.17
$Area(cm^2)$	93.6	96.23	146.3	93.6	96.23	146.3
Q_{Aitken}	60.36	54.12	46.1	56.54	58.57	40.7
Q_{Kajfez}	56.97	54.22	46.25	57.22	59	39.72

the number of iterations, and to compare it with equivalent Euclidean-shaped microstrip patch antennas.

Providing that the field distribution along the radiating aperture and within the cavity region of the antenna does not change as the height is varied, it can be shown that the radiation quality factor has the following expression [18]:

$$Q_r = \frac{2\omega\epsilon_r}{hG/l} K \qquad (4)$$

where h is the patch height, G/l is the conductance per unit length of the radiating aperture, and K is given by

$$K = \frac{\int\int_S |E_{int}|^2 \, ds}{\oint_{perimeter} |E_{int}|^2 \, dl}. \qquad (5)$$

E_{int} is the electric field inside the patch.

Usually, the quality factor due to conductor and dielectric losses is much larger than the radiation quality factor. In this case, the total quality factor depends on the radiation quality factor, and (4) shows that the quality factor is proportional to the inverse of the substrate height.

First of all, the comparison is made with patches of equal area. The methods employed to compute the quality factor Q [15], [16] require the knowledge of the input return loss. The Q of the Koch1, Koch2, Koch3, and Koch4 circular and hexagonal patches has been computed from the measured input return loss. To minimize the effect of dielectric losses, the patches have been built with air as a dielectric. The height of the patches is 5 mm and all of them have an area of 44.8 cm^2.

Table I shows the fundamental resonant frequency at which the quality factor is computed and the computed quality factor calculated with the Aitken [15] and Kajfez [16] methods.

According to the results in Table I, the quality factor is similar among the different iterations when the number of iteration increases. On the other hand, the quality factors displayed by the closest Euclidean versions are much smaller. Nevertheless, it must be noted that the resonant frequency of the Euclidean

patches is higher. In this case, the height of the patch in terms of the wavelength is higher and the radiation losses increase. As it is shown in (4), the result is a reduction of the quality factor. Therefore, to draw relevant conclusions the quality factor of Koch and Euclidean patches with the same resonant frequency must be compared.

To compute the quality factor, the input return loss of the Koch3 and Koch5 patches are measured, together with the input return loss corresponding to the circular patch with the same resonant frequency. The patches are measured for a substrate height of 3.4 mm, and air as a dielectric. In addition, the quality factor computed through the measured input reflection coefficient is compared with the results obtained from the simulated input return loss.

Table II describes the fundamental resonant frequency at which the quality factor is computed, and the computed quality factor calculated with the methods of Aitken and Kajfez. Both methods are applied to simulated and measured data. The differences obtained by each method must be attributed to the different sensitivity of each method to deviations from a truly RLC behavior. No losses are considered in the simulated data.

The first observation is that the measured resonant frequencies and the simulated frequencies are similar. However, the quality factors do not exhibit the same degree of similarity. Despite the discrepancies between measurements and simulations, it can be concluded that the quality factor of the Euclidean patch is smaller than the quality factor of the Koch patch.

In accordance with the (4), when two patches have the same resonant frequency and the same substrate height, the quality factor depends on two parameters: the conductance per unit length of the radiating aperture, and the K factor that is defined by (5). The K factor is the surface integral of the electric field over the patch area divided by the line integral of the electric field around the patch perimeter. One may be tempted to think that the larger perimeter of the Koch patch would reduce the K factor, reducing the quality factor. However, the results reveal that the circular patch displays a lower quality factor than the Koch patch, and that there is no noticeable reduction of the Q when the number of iterations of the prefractal is increased.

In conclusion, the Koch island fractal microstrip antenna resonates at the fundamental mode at a frequency lower than the
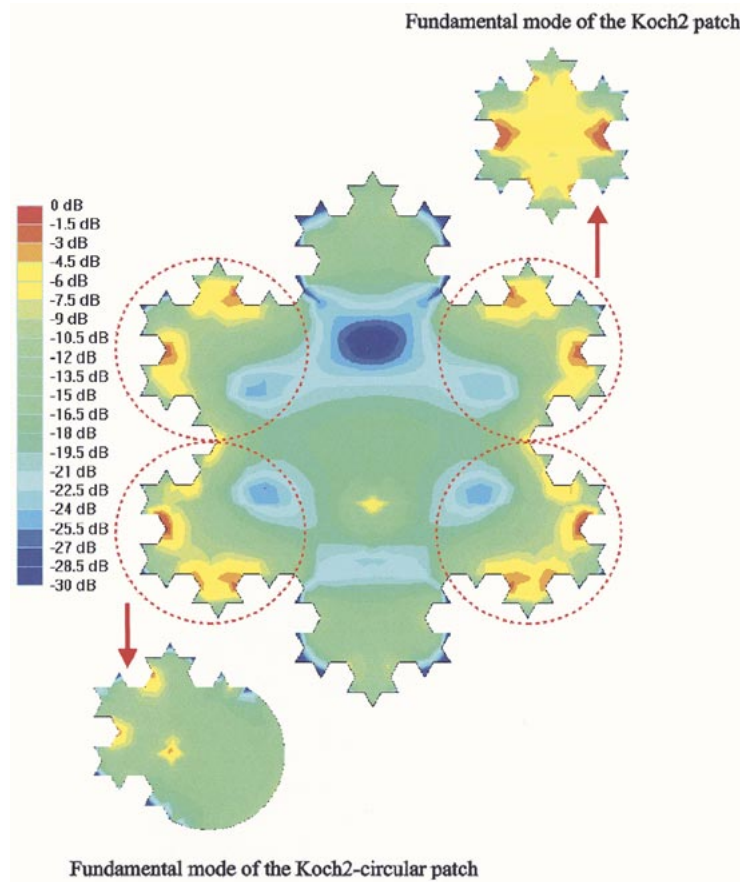
Fig. 6. The electric current density magnitude for the sixth mode of the Koch3 patch. The current is normalized with respect to its maximum and covers a 30-dB dynamic range. It is interesting to note that the red-circled regions have a current density distribution that resembles that of fundamental mode of the Koch2 patch or the Koch2 circular patch, that are also shown for comparison.

equivalent Euclidean patches, such as the circular or hexagonal patch with the same area. Conversely, for a given resonant frequency, the Koch island patch antenna has a smaller area. This can be an interesting feature when it is necessary to minimize conductor losses or expensive materials such as superconductor materials that are employed in the construction of the patch. Nevertheless, this area reduction results in a higher Q for the Koch island patch antenna. When compared with a circular patch antenna resonating at the same frequency, a Q higher by about 17% has been measured in a Koch patch antenna of five iterations. This higher Q results in a smaller bandwidth.

IV. LOCALIZED MODES IN FRACTAL BOUNDARY MICROSTRIP PATCH ANTENNAS

In this section, the existence of high-order localized modes in fractal boundary microstrip antennas and its application are presented. The effect of localization is an important subject in the physics of disordered materials, which has received considerable attention during the last years. A localized state corresponds to a waveform, which is mainly placed in a finite volume whereas a delocalized state occupies an infinite or semi-infinite volume.

The effect of localization for Neumann fractinos is to enhance locally the amplitude of the vibration at the cavity boundary because the boundary region is free to vibrate. The localization is

a consequence of the partially destructive interference of waves reflected by the irregular boundary.

It has been shown that patch antennas with a fractal boundary condition exhibit localized modes [13]. The current is essentially concentrated in an area close to the boundary of the patch. Fig. 6 displays the electric current density magnitude for the sixth mode of the Koch3 patch antenna. The following observations can be made from the current plot. First of all, the current is essentially localized in four regions (red dotted circle) of the patch, which partially resemble the two-iteration version of the Koch island patch scaled by a factor of 1/3. Second, the current density in the four localized regions can be associated with the fundamental mode of the Koch2 patch, but scaled by a factor of 1/3. In Fig. 6, the current distribution at the fundamental mode for a combination of a Koch2 and a circular patch is also shown. It is interesting to observe that it is the high irregularity of the fractal boundary that supports localized current distributions.

Due to the fact that current density maxima are in phase, and the larger electrical size of the patch at this frequency, the radiation pattern presents a higher directivity in comparison with the directivity of the patch at the fundamental mode. The radiation pattern is very similar to the one displayed by an array of 2×2 elements. It should be added that the spacing between localized regions is large in terms of wavelength. The distance between the current maxima is of the order of 1.3λ, so the sidelobe level
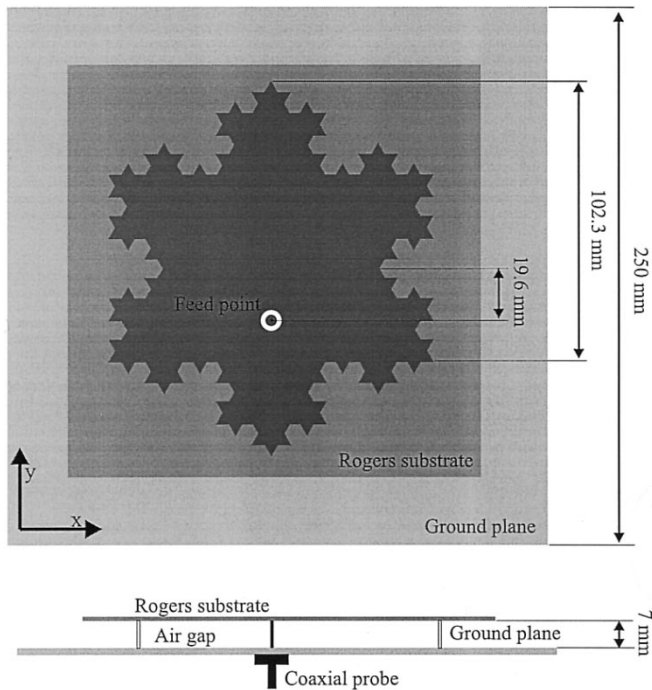
Fig. 7. Koch3 patch antenna geometry. A capacitive gap has been added to compensate for the inductive behavior of the coaxial feed.

should be considerable since the grating lobes are in the visible range. Such property is linked to the fact that the dielectric material used to print the patch has a dielectric permittivity very close to one. It must be stressed that for Euclidean patches such as the rectangular patch, high-order modes present current density maxima that are in opposite phase, and tend to cancel each other's contribution to radiation.

The Koch Island patch antenna geometry is shown in Fig. 7. A three-iteration version of the Koch Island fractal has been built. The fractal patch has been etched on a 0.8-mm substrate with $\epsilon_r = 3.38$. An additional air gap of 7 mm between the substrate and the ground plane is considered.

The patch is fed through a coaxial probe. The inductive effect of the feeding probe is considerable since the separation between the patch surface and the ground plane is high in terms of wavelength ($h/\lambda \sim 0.09$). A capacitive gap is used to properly compensate the probe inductance. The gap is etched on the patch surface and takes the form of an anular gap around the feed probe. The feed point is placed at 19.2 mm from the center of the patch, the internal diameter is 6 mm, and the external diameter is 8 mm.

The measured input impedance and the input reflection coefficient is displayed in Fig. 8. The fractal patch is matched at 50 Ω, the central marker is placed at the minimum input return loss, and the other two markers correspond to the frequencies whose input return-loss level is −14 dB. Therefore, a 12% impedance bandwidth is obtained for an input return-loss level of −14 dB.

The measured main cuts (H-plane and E-plane) are displayed in Fig. 9 for the E_θ and E_ϕ components and the total pattern with a 30-dB dynamic range. The cuts are measured at the central frequency of the operating band, 3.52 GHz. The pattern is broadside for both planes and the beam width is 36.9° at the H-plane
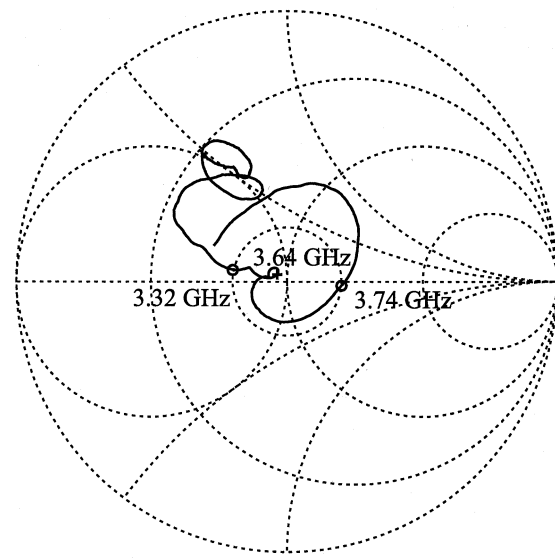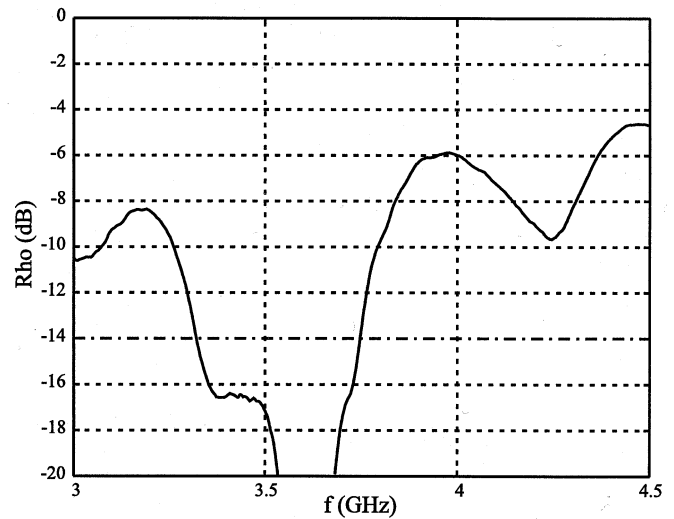
Fig. 8. (a) Measured input impedance of the Koch island patch antenna at the localized mode. (b) Measured input reflection coefficient of the Koch Island patch antenna at the localized mode.

and 27.4° at the E-plane, the directivity is around 12.7 dB. The directivity for the same structure at the fundamental mode is only 9 dB. The fundamental resonant frequency is 1.11 GHz. Therefore, the fact that at the higher order mode the patch is acting as a larger antenna in terms of the wavelength results in a more directive pattern.

V. PERTURBATION OF THE KOCH MICROSTRIP PATCH ANTENNA

The generation of localized modes is the result of the high irregular boundary of the resonator. In order to show that it is possible to design patches with similar properties but with different geometry, the Koch butterfly patch antenna has been analyzed and measured. In Fig. 11, the geometry of the patch is shown. It is essentially obtained by overlapping two Koch island fractals. The Koch butterfly patch is designed to operate in the localized mode that is linked to the fifth resonant mode.
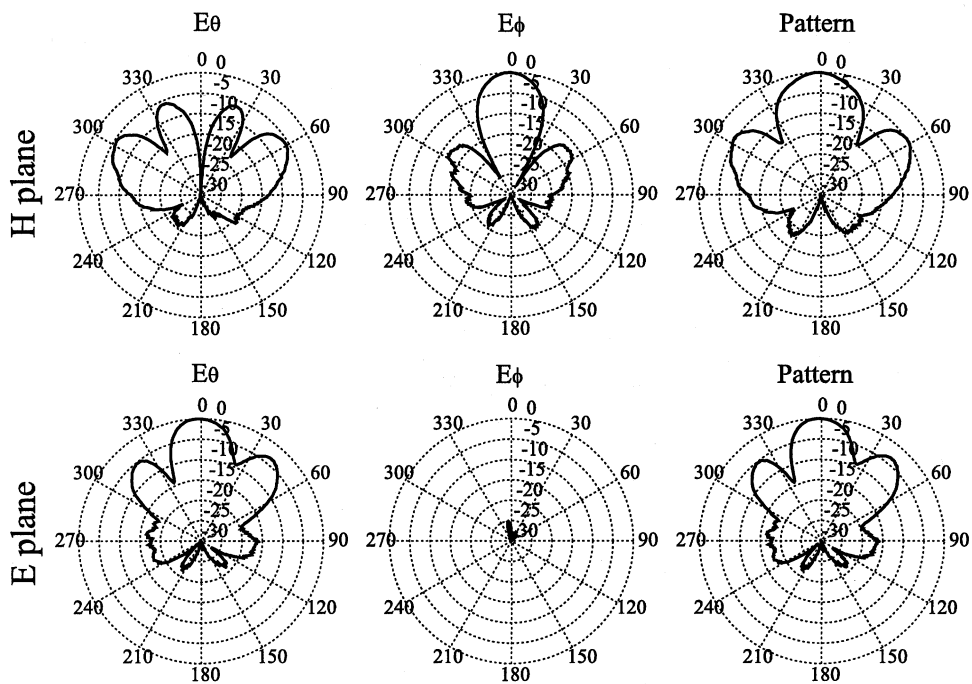
Fig. 9.   Koch island patch radiation pattern main cuts (H-plane and E-plane) measured for the localized mode at 3.52 GHz. The plot shows the E_ϕ and E_θ components, together with the total pattern.
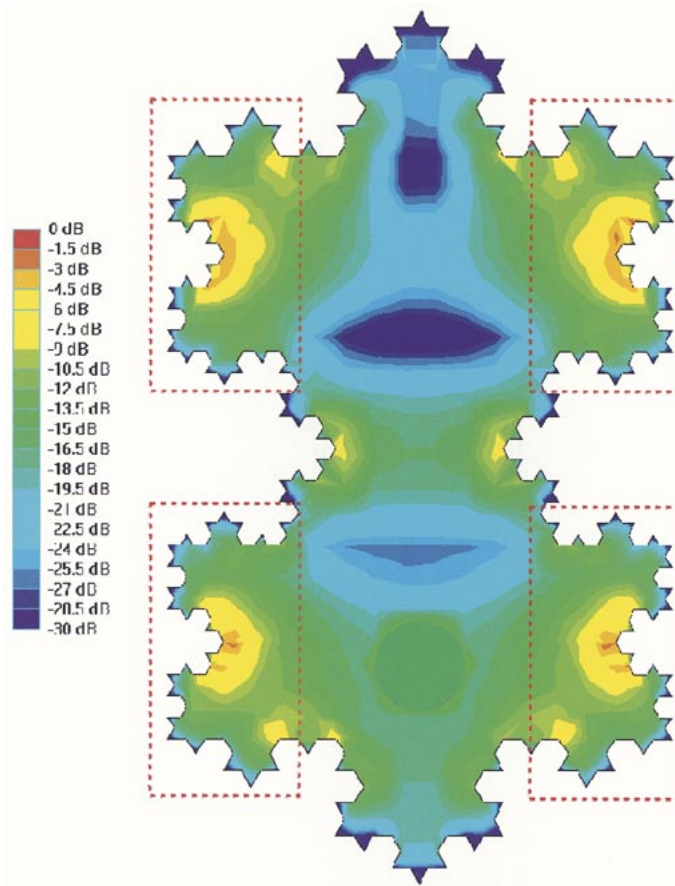

Fig. 10.   The electric current density magnitude for the fifth mode of the Koch3 butterfly patch at 2.81 GHz. The current is normalized with respect to its maximum and covers a 30-dB dynamic range. The red-dotted rectangles enclose the current density maxima.
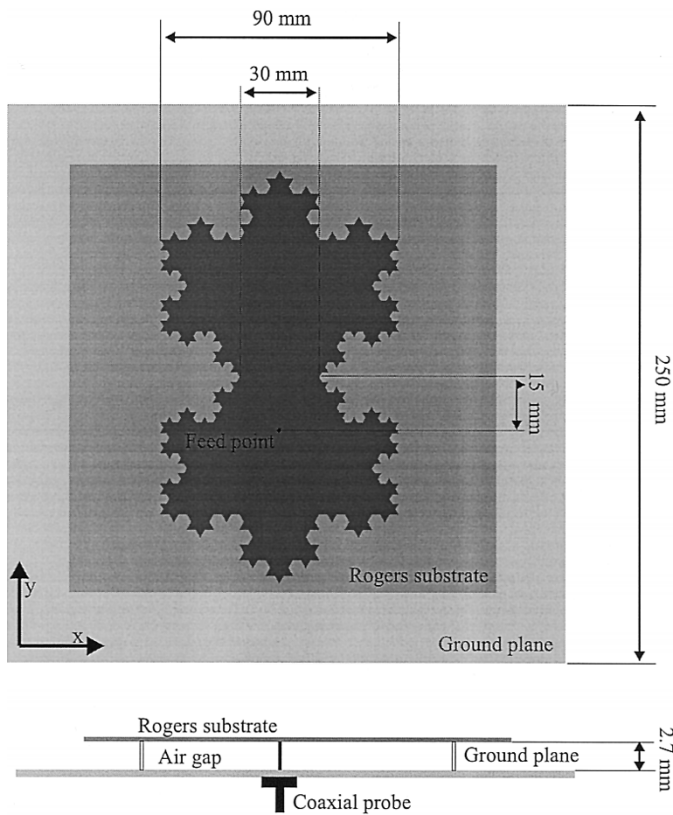
Fig. 11.   Koch butterfly patch geometry.
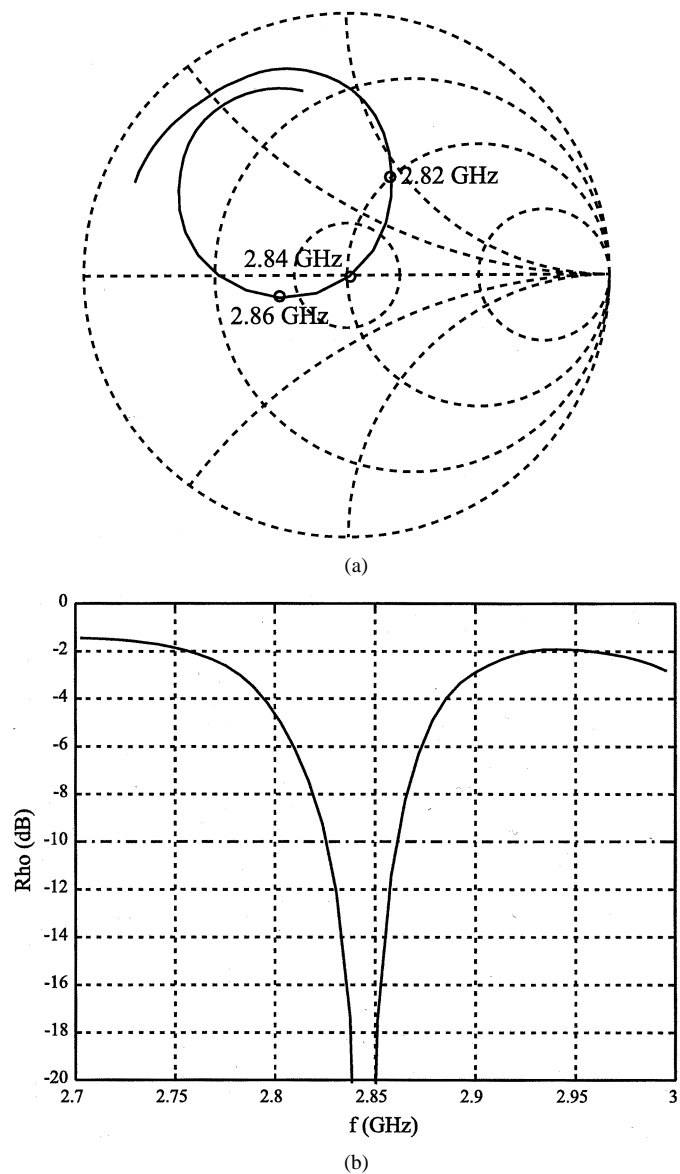

(a)

(b)

Fig. 12.   (a) Measured input impedance of the Koch butterfly patch antenna for the localized mode. (b) Measured input reflection coefficient of the Koch butterfly patch antenna for the localized mode.

The radiation properties of the localized modes corresponding to the Koch3 butterfly are studied. Fig. 10 displays the electric current density magnitude for the fifth resonant mode of the Koch3 butterfly at 2.81 GHz. As in the case of the Koch3 patch, the electrical current is mainly localized in four regions (red dotted rectangles) of the patch.

The Koch butterfly patch antenna geometry is shown in Fig. 11. A three-iteration version of the Koch butterfly fractal has been built. The fractal patch has been etched on a 0.8-mm Rogers substrate with $\epsilon_r = 3.38$. An additional air gap of 2.7 mm between the substrate and the ground plane is considered. The patch is fed through a coaxial probe that is placed at 15 mm from the center point.

The measured input impedance and the input reflection coefficient is displayed in Fig. 12. The fractal patch is matched at 50 Ω, the central marker is placed at the minimum input return loss, and the other two markers corresponds to the frequencies whose input return-loss level is −10 dB.

The measured main cuts (H-plane and E-plane) are displayed in Fig. 13 for the E_θ and E_ϕ components and the total pattern with a 30-dB dynamic range. The cuts are measured at the central frequency of the operating band. To compare the high-directivity mode with the patch behavior at the fundamental mode, the cuts corresponding to the fundamental resonant frequency of the Koch butterfly patch are also represented in Fig. 13. The fundamental mode is a nonlocalized mode since the current is distributed over all the patch surface. The pattern of the localized mode is broadside for both planes, the beam width is

42° at the H-plane and 34° at the E-plane. The sidelobe level at the E-plane is below −10 dB and the directivity is 13.4 dB. It must be remarked that the directivity at the fundamental mode is around 9 dB. Therefore, an increase of almost 4.5 dB is achieved. Such behavior is due to larger electrical dimensions of the Koch3 butterfly patch at the frequency corresponding to the localized mode, and also because the localized density currents are in phase.

The experimental results reveal that the localized current distribution displayed by the fifth resonant mode of the Koch3 butterfly patch results in a patch antenna with a higher directivity than the directivity of classical Euclidean patches. A similar result could be obtained with a 2×2 array of rectangular or circular patches operating at the fundamental frequency. Nevertheless, the fractal perimeter microstrip patch antenna attains a similar performance with simple feeding network, since just one feeding point is required.

Fundamental mode (non-localized), fo=0.81 GHz

Localized mode, fo=2.84 GHz

Fig. 13. Koch butterfly patch radiation pattern main cuts (H-plane and E-plane) measured for the fundamental resonant mode at 0.81 GHz and for the localized mode at 2.84 GHz. The plot shows the E_ϕ and E_θ components, together with the total pattern.

VI. Conclusion

The Koch island fractal boundary microstrip antenna has been numerically and experimentally analyzed. This antenna is a good example of the properties of fractal boundary microstrip antennas. At the fundamental mode, the antenna has a resonant frequency slightly lower than equivalent Euclidean shaped antennas, but with a considerable area reduction. It also has a higher Q that will result in a smaller bandwidth. One of the most interesting properties is the existence of higher order modes that result in directive patterns. Two examples have been presented that exhibit a directivity of the order of 4 dB higher than a patch antenna operating at the resonant frequency. This behavior is obtained with a simple feeding scheme. Therefore, fractal boundary microstrip patch antennas are an interesting alternative in the design of single-fed radiating elements with broadside radiation patterns and with a directivity in the range of 13 dB.

References

[1] C. Puente, J. Romeu, R. Pous, and A. Cardama, "On the behavior of the Sierpinski multiband antenna," *IEEE Trans. Antennas Propagat.*, vol. 46, pp. 517–524, Apr. 1998.

[2] J. Soler and J. Romeu, "Generalized Sierpinski fractal antenna," *IEEE Trans. Antennas Propagat.*, vol. 49, pp. 1237–1239, Aug. 2001.

[3] J. Romeu and Y. Rahmat-Samii, "Fractal FSS: A novel multiband frequency selective surface," *IEEE Trans. Antennas Propagat.*, vol. 48, pp. 713–719, July 2000.

[4] E. Parker and A. N. A. El Sheikh, "Convoluted array elements and reduced size unit cells for frequency-selective surfaces," in *Proc. Inst. Elec. Eng., Pt.H (Microwaves, Optics and Antennas)*, vol. 138, Feb. 1991, pp. 19–22.

[5] C. Puente, J. Romeu, and A. Cardama, "The Koch monopole: A small fractal antenna," *IEEE Trans. Antennas Propagat.*, vol. 48, pp. 1773–1781, Nov. 2000.

[6] ——, "Fractal-shaped antennas," in *Frontiers in Electromagnetics*, D.H. Werner and R. Mittra, Eds. Piscataway, NJ: IEEE Press, 2000.

[7] J. Parron, J. M. Rius, and J. Romeu, "Improving the performance of method of moments for the analysis of fractal antennas," in *Antennes Non-Standard: Techniques et Traitements, Jounées SEE*, Paris, France, Mar. 2000.

[8] B. Sapoval and Th. Gobron, "Vibrations of strongly irregular or fractal resonators," *Phys. Rev. E*, vol. 47, no. 5, pp. 3013–3024, May 1993.

[9] S. Russ, B. Sapoval, and O. Haeberle, "Irregular and fractal resonators with Neumann boundary conditions: Density of states and localization," *Phys. Rev, E*, vol. 55, no. 2, pp. 1413–1421, Feb. 1997.

[10] C. Even, S. Russ, V. Repain, P. Pieranski, and B. Sapoval, "Localizations in fracal drums: An experimental study," *Phys. Rev. Lett.*, vol. 83, no. 4, pp. 726–729, July 26, 1999.

[11] M. L. Lapidus, J. W. Neuberger, R. J. Renka, and C. A. Griffith, "Snowflake harmonics and computer graphics: Numerical computation of spectra on fractal drums," *Int. J. Bifurcation and Chaos*, vol. 6, no. 7, pp. 1185–1210, 1996.

[12] J. Romeu and C. Borja, "Antena microstrip con perímetro fractal o prefractal," Application for Spanish Patent, Application P200 000 238, Jan. 2000.

[13] C. Borja, G. Font, S. Blanch, and J. Romeu, "High directivity fractal boundary microstrip patch antenna," *Electron. Lett.*, vol. 36, no. 9, pp. 778–779, Apr. 27, 2000.

[14] C. Borja and J. Romeu, "Fracton vibration modes in the Sierpinski microstrip patch antenna," in *Proc. IEEE Antennas and Propagation Soc. Int. Symp.*, Boston, MA, July 8–13, 2001, pp. 612–615.

[15] J. E. Aitken, "Swept-frequency microwave Q-factor measurement," *Proc. Inst. Elec. Eng.*, vol. 123, no. 9, pp. 855–861, Sept. 1976.

[16] D. Kajfez and E. J. Hwan, "Q-factor measurement with network analyzer," *IEEE Trans. Microwave Theory Tech.*, vol. MTT-32, pp. 666–670, July 1984.

[17] I. J. Bahl and P. Bhartia, *Microstrip Antennas*. Dedham, MA: Artech House, 1980.

[18] D. M. Pozar and D. H. Schaubert, *Microstrip Antennas: The Analysis and Design of Microstrip Antennas and Arrays*. Piscataway, NJ: IEEE Press, 1995.

Carmen Borja (S'99) was born in Barcelona, Spain, in 1972. She received the Ingeniero degree in telecommunications engineering from the Polytechnic University of Catalonia (UPC), Barcelona, in 1997, and the Ph.D. degree from the UPC in 2001.

From 1997 to 2000, she was with the Electromagnetics and Photonics Engineering group (EEF) at the UPC, where she worked on the development of fractal technology applied to microstrip antennas. Since June 2000, she has been with Fractus S.A., where she holds the position of Project Manager. During 1999, she was working at the Antenna, Research, Analysis, and Measurement Laboratory, University of California, Los Angeles (UCLA) for two months. She holds several patents on fractal and other antenna inventions. Her research interests are fractal, miniature and multiband antennas.

Ms. Borja was awarded the Best Doctoral Thesis in Advanced Mobile Communications 2002 prize by the Colegio Oficial de Ingenieros de Telecomunicación (COIT) and Fundación Airtel-Vodafone. In 1998, the team where she worked at the UPC received the European Information Technology Grand Prize from the European Council for the Applied Science and Engineering (EuroCASE) and the European Commission, for the work in fractal-shaped antennas and their application to cellular telephony.

Jordi Romeu (S'88–M'93) was born in Barcelona, Spain, in 1962. He received the Ingeniero and Doctor Ingeniero degrees in telecommunication engineering, both from the Polytechnic University of Catalonia (UPC), Barcelona, Spain, in 1986 and 1991, respectively.

In 1985, he joined the Electromagnetic and Photonics Engineering Group of the Signal Theory and Communications Department there. Currently, he is Associate Professor at UPC, where he is engaged in research in antenna near-field measurements, antenna diagnostics, and antenna design. He was a Visiting Scholar at the Antenna Laboratory, University of California, Los Angeles, in 1999 supported by a NATO Scientific Program scholarship. He holds several patents and has published papers in the fields of antenna near-field measurements and diagnostics, and in antenna design.

Dr. Romeu was the Grand Winner of the European IT prize awarded by the European Commission for his contributions in the development of fractal antennas in 1998.